PHYSICAL REVIEW B **70**, 165104 (2004)

Three-dimensional photonic crystals by holographic lithography using the umbrella configuration: Symmetries and complete photonic band gaps

D. C. Meisel*
Institut für Nanotechnologie, Forschungszentrum Karlsruhe in der Helmholtz-Gemeinschaft, D-76021 Karlsruhe, Germany

M. Wegener
Institut für Angewandte Physik, Universität Karlsruhe (TH), D-76128 Karlsruhe, Germany

K. Busch
Institut für Theorie der Kondensierten Materie, Universität Karlsruhe (TH), D-76128 Karlsruhe, Germany
and Department of Physics and School of Optics: CREOL & FPCE, University of Central Florida, Orlando, Florida 32816, USA
(Received 20 April 2004; published 13 October 2004)

We present a detailed study of the crystallographic symmetries and band structures of three-dimensional photonic crystals that are amenable to nanofabrication through holographic lithography. For the experimentally preferable umbrella geometry, we identify realistic parameters that lead to structures with complete three-dimensional photonic band gaps. We find a solution, for which the photonic crystals have rhombohedral point symmetry. This solution is a member of the same space group as the celebrated Yablonovite structure and has a similar crystallographic motif. We find a complete photonic band gap with a gap/midgap ratio of 5.8% between the second and third band after silicon inversion at 38% silicon filling fraction. In addition, we identify parameter combinations for which the optimized interference contrast is as large as a factor of 10, rendering the fabrication of this structure possible.

DOI: 10.1103/PhysRevB.70.165104 PACS number(s): 42.70.Qs, 78.66.Sq

I. INTRODUCTION

The large-scale nanofabrication of high-quality three-dimensional (3D) photonic crystals (PC's) with complete photonic band gaps[1,2] (PBG's) at near-infrared and visible frequencies still poses a major challenge to material science. Among the many theoretically suggested structures only a few can actually be manufactured.

Inverse opals offer inexpensive fabrication of large-scale PC's through the self-assembly of colloidal particles into PC templates which are subsequently infilled with high-index materials such as silicon.[3–5] However, the self-organizing nature of this assembly process almost inevitably leads to the formation of unwanted defects, such as missing particles (cavities), dislocations (grain boundaries), etc. In addition, the controlled incorporation of functional elements through suitably designed defect structures in opals remains a challenging problem.

PBG's at infrared frequencies in the layer-by-layer structure[6,7] have recently been realized through combinations of advanced planar semiconductor nanostructuring techniques for individual layers with sophisticated alignment and stacking procedures to combine different layers into 3D PC's.[8–10] These technologically very demanding approaches allow the incorporation of functional elements through controlled modifications in individual layers. However, to date, successful stacking has been reported only for a few layers. This rather limited size leads to a strong coupling between the guiding modes required for the operation of functional elements embedded in these PC's to the leaky modes of the material surrounding the PC structure. As a result, the performance of these functional elements is compromised.

Recently, holographic lithography (HL)[11–13] has emerged as a very promising technique for the inexpensive fabrication of high-quality 3D PC templates. Together with direct laser writing (DLW) approaches,[14] HL offers the attractive possibility of controlled incorporation of functional elements using DLW in a second step.

In HL, a thick photoresist layer is exposed to a multiple-beam interference pattern and subsequently developed. Negative photoresists exhibit a certain exposure dose threshold, above which the photoresist becomes insoluble in the developing process. Therefore, in these materials the spatial distribution of the radiation dose transfers into a corresponding matter distribution. The final result is a porous polymer-air structure, the shape of which is given by the isodose surface for the threshold value. Similarly, for positive photoresists, the underexposed regions remain after development.

To increase the refractive index contrast—which is necessary to obtain complete PBG's—the structures must be infiltrated with a transparent high refractive index material such as, e.g., silicon. Nevertheless, the templates themselves may be utilized for the realization of diffractive elements.

The creation of 3D periodic template structures using HL requires at least four noncoplanar beams[15–17] with five parameters per beam (beam intensity, direction, and polarization state). Within the resulting 20-dimensional parameter space, it is necessary to identify those structures that are doubly connected (a polymer network for mechanical stability of the template and an air network for infilling with high refractive index material) and that will exhibit a PBG after templating. To date, two different four-beam configurations have been discussed[15] (see Fig. 1): (i) The "umbrella" and (b) the "two-planes" or "tetrahedral"[18] configuration. The latter has been discussed theoretically in detail and parameters suitable for complete 3D PBG's have been given explicitly.[19–22] Gap/midgap ratios larger than 20% have been

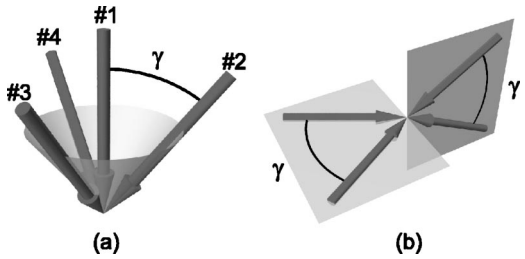

FIG. 1. (a) The umbrella configuration: The central beam (No. 1) is along the axis of a cone with apex angle γ; three side beams (Nos. 2, 3, 4) are equally distributed on the cone. (b) The two-planes geometry: Two pairs of counterpropagating beams in two perpendicular planes.

predicted for a dielectric contrast of 13:1.[19–25]

On the other hand, for the umbrella geometry, a systematic discussion has not been given in the literature. This is very unfortunate because the umbrella configuration is much more convenient from an experimental point of view as all four beams originate within the same half space (except for bcc, see below). Therefore, opaque or absorbing substrates can be used in umbrella configuration, whereas the two-planes geometry requires two beams to pass the substrate before they reach the photoresist layer. Another disadvantage of the counter-propagating beams in the two-planes configuration is that for a given exposure wavelength λ and desired translational symmetry, the lattice constants achievable in the two-planes geometry are generally smaller than those of the umbrella configuration. For instance, the lattice constant $a_{\mathrm{fcc}}=1.12\lambda$ in the face-centered cubic (fcc) case is 2.3 times smaller for the two-planes configuration as compared to the umbrella configuration, for which $a_{\mathrm{fcc}}=2.60\lambda$. In principle, this could be compensated by employing larger exposure wavelengths. However, the availability of photoinitiators currently limits the exposure wavelength to a maximum of about 600 nm in air for single photon absorption. The small lattice constants of the two-planes geometry are undesired because the resulting PBG's or stop bands are correspondingly shifted towards rather short wavelengths, which severely limits the choices for infiltration with high refractive index materials. Furthermore, the small lattice constants of the two-planes configuration are barely compatible with typical photoresist spatial resolutions. In fact, to the best of our knowledge none of the proposed structures in the two-planes geometry has actually been fabricated as a porous template by holographic lithography as of yet.

TABLE I. Angle γ (see Fig. 1) and corresponding lattice constants a_{TS} for the umbrella and the two-planes geometry for the realization of the cubic translational symmetries (TS's). In order to allow a direct comparison of the two geometries, the face-centered cubic lattice constant is given for both configurations although the rhombohedral lattice constant would be a more natural choice for the umbrella geometry. The lattice constants are given in multiples of the exposure wavelength $\lambda=\lambda_0/n_{\mathrm{photoresist}}$ inside the photoresist. For bcc translational symmetry the two geometries coincide.

Umbrella configuration		
TS	γ inside SU-8 layer	cubic lattice constant
sc	$\gamma_{\mathrm{sc}}=\arccos(1/3)\approx 70.53°$	$a_{\mathrm{sc}}=\lambda\sqrt{3}/2\approx 0.87\lambda$
bcc	$\gamma_{\mathrm{bcc}}=\arccos(-1/3)\approx 109.47°$	$a_{\mathrm{bcc}}=\lambda\sqrt{3}/2\approx 0.87\lambda$
fcc	$\gamma_{\mathrm{fcc}}=\arccos(7/9)\approx 38.94°$	$a_{\mathrm{fcc}}=\lambda 3\sqrt{3}/2\approx 2.60\lambda$
two-planes configuration		
TS	γ inside SU-8 layer	cubic lattice constant
bcc	$\gamma_{\mathrm{bcc}}=\arccos(-1/3)\approx 109.47°$	$a_{\mathrm{bcc}}=\lambda\sqrt{3}/2\approx 0.87\lambda$
fcc	$\gamma_{\mathrm{fcc}}=\arccos(-3/5)\approx 126.87°$	$a_{\mathrm{fcc}}=\lambda\sqrt{5}/2\approx 1.12\lambda$

In this paper, we systematically discuss the umbrella configuration for the fabrication of PC templates using HL. We identify parameters that are suitable for obtaining complete 3D PBG's. After giving a brief overview of both the umbrella and the two-planes geometry, we discuss the umbrella configuration in terms of its crystallographic symmetries. Finally, we give explicit examples for structures that would exhibit PBG's at the telecommunication wavelength window at 1.5 μm after infiltration with high refractive index materials such as, e.g., silicon.

II. CRYSTALLOGRAPHIC SYMMETRY ANALYSIS

Table I lists the angles γ required inside the photoresist layer for realizing the three different cubic translational symmetries—simple cubic (sc), face-centered cubic (fcc), and body-centered cubic (bcc)—and their periods in terms of the internal exposure wavelength $\lambda=\lambda_0/n_{\mathrm{photoresist}}$ for both beam geometries. Due to the refraction at the air/photoresist interface, all internal angles γ given in Table I are accessible only by use of immersion systems.[13] The sc symmetry can only be obtained with the umbrella geometry. Note that for bcc translational symmetry in the umbrella configuration the apex angle γ is essentially the same as in the sc case but with the central beam (No. 1) traveling in the opposite direction with respect to the side beams (Nos. 2, 3, 4): $\gamma_{\mathrm{bcc}}-180°=-70.53°=-\gamma_{\mathrm{sc}}$. Indeed, for this apex angle γ_{bcc} the umbrella configuration becomes identical to the corresponding two-planes geometry. Thus, our above reasoning that the umbrella configuration is experimentally advantageous compared to the two-planes geometry (all beams originate within the same half-space) does *not* hold for the bcc case.

It is crucial to note, however, that it is generally insufficient to consider the lattice translational symmetry only. Instead, one has to analyze the symmetry of the individual unit cell, too. For instance, fcc translational symmetry is necessary but not sufficient for the realization of a fcc PhC. In general, for arbitrary polarizations and relative intensities of the four interfering beams, the only point symmetry of the resulting PhC is the identity operation. This reasoning applies to both beam configurations. For the two-planes configuration, the special conditions to ensure certain symmetry properties have been discussed elsewhere.[20–22]

The spatial distribution of the exposure dose $D(\vec{r})$ through the interference of four plane waves with wave vectors $\vec{k}_n$ and amplitude-polarization vectors $\vec{E}_n^0$ can be expressed as a Fourier series[16,13]

$$D(\vec{r}) \propto \left| \sum_{n=1}^{4} \vec{E}_n^0 e^{i(\vec{k}_n \cdot \vec{r} - \omega t)} \right|^2 = \sum_{n,m=1}^{4} a_{nm} e^{i\vec{G}_{nm} \cdot \vec{r}}$$

$$= \sum_{n=1, m \geqslant n}^{4} \mathrm{Re}\{a_{nm} e^{i\vec{G}_{nm} \cdot \vec{r}}\}(2 - \delta_{nm}), \quad (1)$$

where we have introduced

$$\vec{G}_{nm} := \vec{k}_n - \vec{k}_m = -\vec{G}_{mn}, \quad (2)$$

$$a_{nm} := \vec{E}_n^0 \cdot \vec{E}_m^{0^*} = a_{mn}^*. \quad (3)$$

The reciprocal lattice vectors $\vec{G}_{nm}$ for which a_{nm} is nonzero fully determine the translational symmetry of the interference pattern. The (generally complex) form factors a_{nm} result from the relative amplitudes and polarizations of the incident laser beams. In combination with $\vec{G}_{nm}$ they determine the shape of the so-called motif of the crystal structure, i.e., the explicit shape of the resist inside an individual unit cell. Then, the overall point symmetry of the structure is the maximal point symmetry common to both, the lattice and the motif. In addition, we would like to note that constant phase factors of the four beams, i.e., $\vec{E}_n^0 \rightarrow \exp(\mathrm{i}\phi_n)\vec{E}_n^0$, merely shift the interference pattern in space and, therefore, do not affect the structure's symmetry properties. For simplicity, we have omitted these factors in the remainder of the manuscript, so that real and complex $\vec{E}_n^0$ correspond to linearly and elliptically polarized light, respectively.

To study the symmetry properties of the exposure dose distribution $D(\vec{r})$ in Eq. (1), one can compare its Fourier series (1) to certain Fourier series with well-known symmetry properties.[20] Such Fourier series are extensively used and discussed in the crystallographic literature.[26] These so-called geometric structure factors $F_{hkl}^{\mathcal{N}}$ are usually given in their respective crystallographic coordinate system[26] and care has to be exerted when translating the results to real space (Cartesian) coordinates. Altogether, there are 230 space groups describing all the inequivalent symmetries that 3D periodic structures may exhibit. More precisely, for space group No. $\mathcal{N}$, there exists a geometric structure factor $F_{hkl}^{\mathcal{N}}$ which is invariant under the symmetry operations of the corresponding space group and is written as[26]

$$F_{hkl}^{\mathcal{N}} = A_{hkl}^{\mathcal{N}} + iB_{hkl}^{\mathcal{N}}, \quad (4)$$

where

$$A_{hkl}^{\mathcal{N}} = \sum_{\sigma=1}^{g^{\mathcal{N}}} \cos[2\pi \vec{h}^{\mathrm{T}}(\mathbf{P}_\sigma^{\mathcal{N}} \vec{r}_{\mathrm{r}} + \vec{t}_\sigma^{\mathcal{N}})]$$

$$B_{hkl}^{\mathcal{N}} = \sum_{\sigma=1}^{g^{\mathcal{N}}} \sin[2\pi \vec{h}^{\mathrm{T}}(\mathbf{P}_\sigma^{\mathcal{N}} \vec{r}_{\mathrm{r}} + \vec{t}_\sigma^{\mathcal{N}})].$$

Here, the superscript T denotes transpositions and $\mathbf{P}_\sigma^{\mathcal{N}}$ and $\vec{t}_\sigma^{\mathcal{N}}$ are, respectively, rotational and translational parts of the σth symmetry operation of space group No. $\mathcal{N}$. In addition, $g^{\mathcal{N}}$ is the number of general Wyckoff positions in the unit cell of space group $\mathcal{N}$ and $\vec{h}^{\mathrm{T}} = (hkl)(h,k,l \in \mathcal{Z})$ is the "diffraction vector" of (integer) Miller indices h,k,l allowed by space group No. $\mathcal{N}$. Finally, the vector $\vec{r}_r^{\mathrm{T}} = (x_r, y_r, z_r)$ denotes the position vector $\vec{r}^{\mathrm{T}}$ with respect to the basis set $\{\vec{a}_1, \vec{a}_2, \vec{a}_3\}$ of crystal axes of space group No. $\mathcal{N}$ which—in general—is not a Cartesian coordinate system:

$$\vec{r}^{\mathrm{T}} = (x,y,z) = x_r\vec{a}_1 + y_r\vec{a}_2 + z_r\vec{a}_3. \quad (5)$$

Here (x,y,z) are the corresponding real space (Cartesian) coordinates of the position vector.

In what follows, we will determine the requirements for the four interfering beams to obtain certain desired crystallographic symmetries in umbrella configuration and will analyze the limitations of this geometry. This is facilitated by expanding the exposure dose $D(\vec{r})$ in Eq. (1) in terms of the real and imaginary part of certain geometric structure factors $F_{hkl}^{\mathcal{N}} = A_{hkl}^{\mathcal{N}} + iB_{hkl}^{\mathcal{N}}$ (4). To this end, the dose (1) has to be represented in an appropriate coordinate system. Any set of three linearly independent reciprocal lattice vectors taken from the 12 off-diagonal $\vec{G}_{nm}$ can serve as basis to span the reciprocal lattice which, for the umbrella configuration, is rhombohedral.

Following the crystallography conventions, a rhombohedral lattice is described by three basis vectors which are of equal length and enclose the same angle with each other. This applies to $\vec{G}_{12} \equiv \vec{b}_1$, $\vec{G}_{13} \equiv \vec{b}_2$, and $\vec{G}_{14} \equiv \vec{b}_3$ which are, therefore, chosen as reciprocal basis vectors. They span a rhombohedral reciprocal lattice which corresponds to a rhombohedral lattice in real space with basis vectors $\vec{a}_i = 2\pi \vec{b}_j \times \vec{b}_k / |\vec{b}_1 \cdot (\vec{b}_2 \times \vec{b}_3)|$, where (i,j,k) is a cyclic permutation of (1,2,3). In contrast to Ref. 20, we rewrite the exposure dose $D(\vec{r})$ (1) in rhombohedral crystal coordinates, thus facilitating a comparison of coefficients

$$\begin{aligned}
\tilde{D}(\vec{r}_{\mathrm{r}}) \propto\ & (a_{11} + a_{22} + a_{33} + a_{44})/2 \\
& + \mathrm{Re}\{a_{12}\}\cos(2\pi x_{\mathrm{r}}) - \mathrm{Im}\{a_{12}\}\sin(2\pi x_{\mathrm{r}}) \\
& + \mathrm{Re}\{a_{13}\}\cos(2\pi y_{\mathrm{r}}) - \mathrm{Im}\{a_{13}\}\sin(2\pi y_{\mathrm{r}}) \\
& + \mathrm{Re}\{a_{14}\}\cos(2\pi z_{\mathrm{r}}) - \mathrm{Im}\{a_{14}\}\sin(2\pi z_{\mathrm{r}}) \\
& + \mathrm{Re}\{a_{32}\}\cos[2\pi(+x_r - y_r)] \\
& - \mathrm{Im}\{a_{32}\}\sin[2\pi(+x_r - y_r)] \\
& + \mathrm{Re}\{a_{43}\}\cos[2\pi(+y_r - z_r)] \\
& - \mathrm{Im}\{a_{43}\}\sin[2\pi(+y_r - z_r)] \\
& + \mathrm{Re}\{a_{24}\}\cos[2\pi(-x_r + z_r)] \\
& - \mathrm{Im}\{a_{24}\}\sin[2\pi(-x_r + z_r)]. \quad (6)
\end{aligned}$$

The spatially constant term in Eq. (6) corresponds to a homogeneous background illumination which is invariant under any symmetry operation. To enable the expansion of Eq. (6) in terms of the $F_{hkl}^{\mathcal{N}}$ they, too, have to be represented in the rhombohedral system ($F_{hkl}^{\mathcal{N}} \rightarrow \tilde{F}_{hkl}^{\mathcal{N}}$). The expansion of the exposure dose $\tilde{D}(\vec{r}_r)$ in terms of the $\tilde{A}_{hkl}^{\mathcal{N}}$ and $\tilde{B}_{hkl}^{\mathcal{N}}$ with expansion coefficients $\alpha_{hkl}^{\mathcal{N}}$ and $\beta_{hkl}^{\mathcal{N}}$ then reads as

TABLE II. The geometric structure factors $\tilde{F}^{\mathcal{N}}_{hkl}=\tilde{A}^{\mathcal{N}}_{hkl}+i\tilde{B}^{\mathcal{N}}_{hkl}$ of the seven rhombohedral space groups as given in the rhombohedral coordinate system (Ref. 26). For convenience, common prefactors are omitted, since they do not affect the symmetry. The following abbreviations are used: $E(c+c+c)=c(hkl)+c(lhk)+c(klh)$, $O(c+c+c)=c(khl)+c(lkh)+c(hlk)$, $E(s+s+s)=s(hkl)+s(lhk)+s(klh)$, and $O(s+s+s)=s(khl)+s(lkh)+s(hlk)$, where $c(hkl)=\cos[2\pi(hx_r+ky_r+lz_r)]$ and $s(lkh)=\sin[2\pi(lx_r+ky_r+hz_r)]$, etc. The capital prefixes E and O represent even and odd permutations of hkl, respectively, with x_r, y_r, and z_r at fixed positions within the sine and cosine arguments.

$\mathcal{N}$	$\tilde{A}^{\mathcal{N}}_{hkl}$	$\tilde{B}^{\mathcal{N}}_{hkl}$
146	$E(c+c+c)$	$E(s+s+s)$
148	$E(c+c+c)$	0
155	$E(c+c+c)+O(c+c+c)$	$E(s+s+s)-O(s+s+s)$
160	$E(c+c+c)+O(c+c+c)$	$E(s+s+s)+O(s+s+s)$
161	for $h+k+l$ even $E(c+c+c)+O(c+c+c)$ for $h+k+l$ odd $E(c+c+c)-O(c+c+c)$	for $h+k+l$ even $E(s+s+s)+O(s+s+s)$ for $h+k+l$ odd $E(s+s+s)-O(s+s+s)$
166	$E(c+c+c)+O(c+c+c)$	0
167	for $h+k+l$ even $E(c+c+c)+O(c+c+c)$ for $h+k+l$ odd $E(c+c+c)-O(c+c+c)$	for $h+k+l$ even 0 for $h+k+l$ odd 0

$$\tilde{D}\propto\sum_{hkl}\alpha^{\mathcal{N}}_{hkl}\tilde{A}^{\mathcal{N}}_{hkl}+\sum_{hkl}\beta^{\mathcal{N}}_{hkl}\tilde{B}^{\mathcal{N}}_{hkl}, \tag{7}$$

where the set of Miller indices (hkl) runs over all values allowed by spacegroup No. $\mathcal{N}$.

A. General rhombohedral symmetry

Based on the fabricational advantages provided by the umbrella configuration discussed in Sec. I, we concentrate on the corresponding seven rhombohedral space groups. This means that the numbers of space groups that may appear in expansion (7) is considerably reduced and only space groups Nos. 146($R3$), 148($R\bar{3}$), 155($R32$), 160($R3m$), 161($R3c$), 166($R\bar{3}m$), and 167($R\bar{3}c$) remain.[26] The associated geometric structure factors $\tilde{F}^{\mathcal{N}}_{hkl}$ are listed in Table II. To facilitate the comparison with the exposure dose, these structure factors are given in the rhombohedral crystal system which is the natural system for the umbrella configuration.

To find conditions for the form factors $\mathrm{Re}\{a_{nm}\}$ and $\mathrm{Im}\{a_{nm}\}$ in Eq. (6) to realize an interference pattern with prescribed rhombohedral symmetry, we compare the function (6) with Table II. The structure of the trigonometric arguments in Eq. (6) is such that the coordinates appear either as isolated (i.e., x_r, y_r, and z_r) or as pairwise differences (i.e., x_r-y_r, y_r-z_r, and $-x_r+z_r$). Therefore, it is sufficient to consider in Table II only ($h=\eta$, $k=0$, $l=0$) and ($h=\eta$, $k=\overline{\eta}$, $l=0$). We require $\eta=1$ for space groups Nos. 146, 148, 155, 160, and 166; for space groups Nos. 161 and 167 the lowest nonvanishing contributions require $\eta=2$ which are duplicates of Nos. 160 and 166, respectively, for $\eta=1$ but with doubled spatial frequency. The trigonometric functions $\tilde{A}^{\mathcal{N}}_{hkl}$ and $\tilde{B}^{\mathcal{N}}_{hkl}$ in Table II are supplied only as $(c+c+c)$ and $(s+s+s)$. In turn, this implies in Eq. (6) that the conditions

$$\mathrm{Re}\{a_{12}\}=\mathrm{Re}\{a_{13}\}=\mathrm{Re}\{a_{14}\}=:u, \tag{8a}$$

$$\mathrm{Re}\{a_{32}\}=\mathrm{Re}\{a_{43}\}=\mathrm{Re}\{a_{24}\}=:v, \tag{8b}$$

$$\mathrm{Im}\{a_{12}\}=\mathrm{Im}\{a_{13}\}=\mathrm{Im}\{a_{14}\}=:p, \tag{8c}$$

$$\mathrm{Im}\{a_{32}\}=\mathrm{Im}\{a_{43}\}=\mathrm{Im}\{a_{24}\}=:q \tag{8d}$$

must be satisfied. With Eqs. (8a)–(8d), $\tilde{D}(\vec{r}_r)$ (6) reads

$$\begin{aligned}\tilde{D}(\vec{r}_r)\propto{}&(a_{11}+a_{22}+a_{33}+a_{44})/2\\&+u\{\cos(2\pi x_r)+\cos(2\pi y_r)+\cos(2\pi z_r)\}\\&+v\{\cos[2\pi(x_r-y_r)\}+\cos[2\pi(y_r-z_r)]\\&+\{\cos[2\pi(-x_r+z_r)]\}\\&-p\{\sin(2\pi x_r)+\sin(2\pi y_r)+\sin(2\pi z_r)\}\\&-q\{\sin[2\pi(x_r-y_r)]\\&+\sin[2\pi(y_r-z_r)]+\sin[2\pi(-x_r+z_r)]\}.\end{aligned} \tag{9}$$

As a result of the foregoing analysis, we have reorganized the 20-dimensional parameter space of a general four-beam interference setup into a form suitable for an analysis of the umbrella configuration. The apex angle γ determines the translational lattice and the relations (8a)–(8d) determine the point symmetry. In addition, we have found that for arbitrary values of (u,v,p,q), the exposure dose $\tilde{D}(\vec{r}_r)$ (9) in umbrella configuration can be completely represented by the rhombohedral space group with lowest symmetry, i.e., by space group No. 146 alone. Thus, expansion (7) is given as

$$\tilde{D}(\vec{r}_r)\propto u\tilde{A}^{\mathrm{No.146}}_{100}+v\tilde{A}^{\mathrm{No.146}}_{1\bar{1}0}-p\tilde{B}^{\mathrm{No.146}}_{100}-q\tilde{B}^{\mathrm{No.146}}_{1\bar{1}0}. \tag{10}$$

Further restrictions on (u,v,p,q) result in higher symmetries: If at least q is zero, i.e., $(u,v,p,0)$, the resulting structures belong to space group No. 160. For structures consistent with space group No. 155, $(u,v,0,q)$ is required. Space group Nos. 148, 166 which in contrast to the other rhombohedral groups contain inversion symmetry may be obtained through $(u,v,0,0)$.

Furthermore, we would like to note that the case $u=p=0$, i.e., $(0,v,0,q)$ implies that the contributions of the central beam to the interference pattern are canceled out, so it is effectively absent. This effective three-beam interference pattern results in two-dimensional structures, with a triangular lattice within the film.

B. Cubic symmetry

Special cases of the rhombohedral lattices are the three cubic lattices sc, bcc, and fcc (see Table I). There are 36

cubic space groups (Nos. 195-230) and we discuss below their relation to the general rhombohedral structure (10).

1. Simple cubic symmetry

If in space group No. 166, v is made to vanish, i.e., $(u,0,0,0)$, and if the apex angle is set to $\gamma=\gamma_{sc}=\arccos(1/3)\approx 70.53°$, the resulting structures belong to the (simple) cubic space group No. 221 ($Pm\bar{3}m$) which is a supergroup to space group No. 166. For this apex angle, the rhombohedral crystal coordinate system becomes a Cartesian coordinate system

$$D(\vec{r}) \propto uA_{100}^{\mathrm{No.221}} = u[\cos(2\pi x)+\cos(2\pi y)+\cos(2\pi z)]. \tag{11}$$

Simple cubic structures with a complete PBG are, for instance, the scaffold structure.[27] The above structure (11) is known as the nodal approximation to Schwarz's triply periodic minimal P surface.[28,29] For this structure, a complete PBG with a gap/midgap ratio of 10% has been predicted for silicon infiltration[20,22] in agreement with our calculations (not shown). Unfortunately, the currently available immersion systems make the realization of the required apex angle of $\gamma_{sc}\approx 70.53°$ *inside* the photoresist rather challenging.

2. Body-centered cubic symmetry

Structures with $(u,u,0,0)$ and $\gamma=\gamma_{bcc}\approx 109.47°$ exhibit the bcc symmetry of space group No. 229 ($I\,m\bar{3}m$):

$$\begin{aligned}\tilde{D}(\vec{r}_r) &\propto u\tilde{A}_{\bar{1}10}^{\mathrm{No.229}}\\ &\propto u\{\cos(2\pi x_r)+\cos(2\pi y_r)+\cos(2\pi z_r)\\ &\quad+\cos[2\pi(x_r-y_r)]+\cos[2\pi(y_r-z_r)]\\ &\quad+\cos[2\pi(-x_r+z_r)]\}.\end{aligned} \tag{12}$$

The representation of Eq. (12) in the cubic crystal coordinate system which coincides with the Cartesian coordinates is

$$\begin{aligned}A_{\bar{1}10}^{\mathrm{No.229}} &\propto \cos[2\pi(x+y)]+\cos[2\pi(y+z)]+\cos[2\pi(x+z)]\\ &\quad+\cos[2\pi(x-y)]+\cos[2\pi(y-z)]\\ &\quad+\cos[2\pi(-x+z)].\end{aligned} \tag{13}$$

This bcc structure (13) has also been mentioned in Ref. 22. No PBG has been found and this has been attributed to the fact that the structure is too symmetric. By choosing another set of form factors, a structure of lower symmetry but with a complete PBG is obtained.[22] In fact the result is a distorted version of the nodal approximation to Schwarz's triply periodic minimal D surface[20,28] (shrinked by $\sqrt{2}$ along the [001] direction) with tetragonal overall symmetry and the relative width of the gap reduces from 24 to 21%.[22]

For $(0,0,p,p)$ and $\gamma=\gamma_{bcc}\approx 109.47°$ structures with bcc overall symmetry but without inversion symmetry, namely that one of No. 214 ($I4_132$) are obtained. The nodal approximation to Schoen's triply periodic minimal G surface (gyroid) corresponds to that case.[20,30]:

$$\begin{aligned}B_{110}^{\mathrm{No.214}} &= B_{\bar{1}10}^{\mathrm{No.214}}\\ &\propto \sin[2\pi(x+y)]+\sin[2\pi(y+z)]+\sin[2\pi(x+z)]\\ &\quad+\sin[2\pi(x-y)]+\sin[2\pi(y-z)]\\ &\quad+\sin[2\pi(-x+z)].\end{aligned} \tag{14}$$

Here, we want to note that for all bcc structures including the ones above, the umbrella configuration becomes equivalent to the two-planes geometry and, consequently, their fabrication faces the challenges discussed in Sec. I.

3. Face-centered cubic symmetry

It is possible to generate structures with fcc translational symmetry by choosing $\gamma=\gamma_{fcc}\approx 38.94°$. In fact, these structures are amenable to nanofabrication through appropriate immersion systems.[13] However, there is no possibility to obtain structures with fcc overall symmetry by using the umbrella configuration; the structure remains rhombohedral. This originates in the absence of a trigonometric function with argument $(x_r+y_r+z_r)$ in Eq. (6), which suggests that a fourfold rotation axis required for fcc overall symmetry is missing in this geometry.

Nevertheless, these rhombohedral structures with fcc translational symmetry are rather interesting because (i) they can actually be fabricated and (ii) their photonic band structure exhibits a PBG as will be shown in Sec. IV. At this point, we want to mention that other well-known structures with rhombohedral overall symmetry are the Yablonovite[31] and the A7 structures.[32] Both structures exhibit complete PBG's.

In the remainder of this manuscript, we restrict ourselves to the case of $(u,0,0,0)$ and $\gamma=\gamma_{fcc}\approx 38.94°$ and discuss fabricational issues of the associated templates and the corresponding photonic bandstructures after infilling of silicon. The resulting structures belong to space group No. 166 ($R\bar{3}m$). In the corresponding cubic crystal coordinate system (Cartesian system), the exposure dose becomes

$$\begin{aligned}D(\vec{r}) &\propto uA_{100}^{\mathrm{No.166}}\\ &= u\{\cos[2\pi(x+y-z)]+\cos[2\pi(x-y+z)]\\ &\quad+\cos[2\pi(-x+y+z)]\}.\end{aligned} \tag{15}$$

C. Balanced structures

The exposure dose $\tilde{D}(\vec{r}_r)$ (9) is composed of a bias $b:=(a_{11}+a_{22}+a_{33}+a_{44})/2$ and a spatially varying part $\tilde{d}(\vec{r}_r)$. For a *negative* photoresist with threshold $(b+\Delta)$, the material remaining after illumination is located at positions where the condition

$$\tilde{D}(\vec{r}_r) \propto b+\tilde{d}(\vec{r}_r) \geqslant b+\Delta \tag{16}$$

is fulfilled.

For $v=q=0$ we have

$$\tilde{d}(\vec{r}_r) = +u[\cos(2\pi x_r)+\cos(2\pi y_r)+\cos(2\pi z_r)] - p[\sin(2\pi x_r)+\sin(2\pi y_r)+\sin(2\pi z_r)]$$

such that $\tilde{d}(\vec{r}_r)=-\tilde{d}(\vec{r}_r+\vec{T}_{111})$ with $\vec{T}_{111}=(0.5,0.5,0.5)$. This is a shift by half of the body diagonal of the rhombohedral unit cell. This relation holds for all allowed apex angles γ.

Therefore, for each point in space which fulfills condition (16), there is a corresponding point shifted by $\vec{T}_{111}$ for which

$$\tilde{D}(\vec{r}_r+\vec{T}_{111}) \propto b+\tilde{d}(\vec{r}_r+\vec{T}_{111}) \leqslant b-\Delta \tag{17}$$

holds. Equation (17) can be understood as follows: If a *positive* resist with threshold $(b-\Delta)$ is exposed to the same interference pattern D, we obtain an identical structure as for the above *negative* resist, simply shifted by $\vec{T}_{111}$. For $\Delta=0$, the filling fraction is 0.5 and the surface of the structure is a so-called "balance surface" dividing space into two congruent regions.[33]

The pores for the filling fraction f have the same shape as the photoresist structure with $(1-f)$. To fabricate a single-infiltration sample with filling fraction f one has the choice to use either a positive or a negative resist. Both templates with filling fraction $(1-f)$ result in the same shape of the infiltrated material.

III. FABRICATION ISSUES

The free choice of the four parameters (u,v,p,q) in Eqs. (8a)–(8d) corresponds to a large variety of structures. In this section we derive the beam polarizations and intensities required for the fabrication of structures with the above discussed symmetries and complete PBG's. In addition, we consider the possibility to optimize the interference contrast which is a parameter of practical importance for the quality of the fabricated templates.

To keep the discussion limited, we restrict ourselves to $p=q=v=0$ in (10), i.e., $(u,0,0,0)$, as this is the simplest case for useful 3D structures (see Secs. II B 1 and II B 3). Thus we have excluded bcc overall symmetry, see Eq. (12). In what follows we will further restrict our discussion to $\gamma=\gamma_{sc}$, i.e., structures with sc overall symmetry and $\gamma=\gamma_{fcc}$, i.e., rhombohedral structures with fcc translational symmetry.

$p=q=0$ implies real form factors a_{nm} (8c) and (8d). This is fulfilled if all four polarization vectors $\vec{E}_n^0$ are real [see Eq. (3)] and, therefore, corresponds to linearly polarized beams. It is then convenient and transparent to describe the linear polarizations by beam-specific cylinder coordinates (ρ_n,θ_n) with cylinder axis $\vec{k}_n$; we use the conventions $\rho_n\epsilon(-\infty,+\infty)$ and $\theta_n\epsilon[0,\pi)$:

$$\vec{E}_n^0=\rho_n[\hat{\vec{s}}_n\sin(\theta_n)+\hat{\vec{p}}_n\cos(\theta_n)]. \tag{18}$$

For $n=2,3,4$ the unity vectors $\hat{\vec{s}}_n$ and $\hat{\vec{p}}_n$ are pointing in the direction of the s and p components of $\vec{E}_n^0$ with respect to the plane spanned by $\vec{k}_1$ and $\vec{k}_n$:

$$\hat{\vec{s}}_n:=\frac{\vec{k}_n\times\vec{k}_1}{|\vec{k}_n\times\vec{k}_1|} \quad \text{for} \quad n=2,3,4, \tag{19}$$

$$\hat{\vec{p}}_n:=\frac{\vec{k}_n\times\hat{\vec{s}}_n}{|\vec{k}_n\times\hat{\vec{s}}_n|} \quad \text{for} \quad n=1,2,3,4. \tag{20}$$

For the central beam, traveling normal to the photoresist layer, for definiteness, we define $\hat{\vec{s}}_1:=\hat{\vec{s}}_2$. The intensity I_n of beam n is proportional to ρ_n^2 and the direction of the polarization is encoded into the angle θ_n enclosed by the vectors $\vec{E}_n^0$ and $\hat{\vec{p}}_n$.

Under these conditions, Eqs. (8a) and (8b) read

$$\mathrm{Re}\{a_{12}\}=\vec{E}_1^0\cdot\vec{E}_2^0=u, \tag{21a}$$

$$\mathrm{Re}\{a_{13}\}=\vec{E}_1^0\cdot\vec{E}_3^0=u, \tag{21b}$$

$$\mathrm{Re}\{a_{14}\}=\vec{E}_1^0\cdot\vec{E}_4^0=u, \tag{21c}$$

$$\mathrm{Re}\{a_{32}\}=\vec{E}_3^0\cdot\vec{E}_2^0=0, \tag{22a}$$

$$\mathrm{Re}\{a_{43}\}=\vec{E}_4^0\cdot\vec{E}_3^0=0, \tag{22b}$$

$$\mathrm{Re}\{a_{24}\}=\vec{E}_2^0\cdot\vec{E}_4^0=0. \tag{22c}$$

Equations (22a)–(22c) suggest that the polarization directions of the side beams (Nos. 2, 3, 4) are pairwise perpendicular to each other and, therefore, do not interfere with each other.

Inserting Eq. (18) into Eqs. (22a)–(22c) has the remarkably simple result

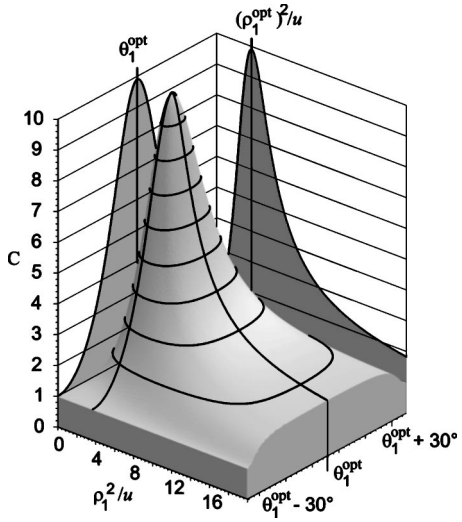

FIG. 2. Dependence of the contrast C of the interference pattern (10) for $(u,v,p,q)=(u,0,0,0)$ on the central beam polarization direction $\theta_1-\theta_1^{opt}$ and $\rho_1^2/u\propto I_1/u$. While θ_1^{opt} (27) depends on the apex angle γ, $(\rho_1^{opt})^2/u=\sqrt{27/2}$ does not depend on γ (29). For sc overall symmetry ($\gamma_{sc}=70.54°$) we find ($\theta_1^{opt}=75.52°$) and for rhombohedral overall symmetry with fcc translational symmetry ($\gamma_{fcc}=38.94°$) $\theta_1^{opt}=28.96°$.

TABLE III. The maximum contrast $C^{\max}$ for sc and fcc translational symmetry (TS) and the corresponding experimental parameters θ_n^{opt} and $I_n^{\text{opt}} \propto (\rho_n^{\text{opt}})^2$ for the umbrella configuration.

TS	$C^{\max}$	θ_1^{opt}	$\theta_{2,3,4}$	I_1^{opt}	I_2^{opt}	I_3^{opt}	I_4^{opt}
sc	9.90	75.52°	52.24°	1	0.11	0.44	0.44
fcc	9.90	28.96°	23.28°	1	0.11	0.44	0.44

$$\theta_{2,3,4} := \theta_2 = \theta_3 = \theta_4 = \pm \arccos\left(\frac{1}{\sqrt{3}\sin(\gamma)}\right). \quad (23)$$

As a consequence, Eqs. (22a)–(22c) require the apex angles γ to lie within the interval

$$\gamma \epsilon [\arcsin(1/\sqrt{3}), \pi - \arcsin(1/\sqrt{3})] = [35.26\,°, 144.74\,°].$$

The ± sign in Eq. (23) has no relevance for the symmetry of the structure. Following our conventions for the θ_n ranges, we choose the + sign. Then, Eq. (23) implies that all three side beams have to be polarized along the same direction relative to their individual *s* and *p* directions.

Inserting (23) into Eqs. (21a)–(21c) allows us to determine ρ_2, ρ_3, and ρ_4 in terms of ρ_1. For ρ_2 we obtain

$$\rho_2 \cdot \rho_1 = u \frac{\sqrt{3}\sin(\gamma)}{\sin(\theta_1)\sqrt{3\sin^2(\gamma) - 1} + \cos(\theta_1)\cos(\gamma)}, \quad (24)$$

and corresponding expressions for ρ_3 and ρ_4 are obtained by replacing θ_1 in Eq. (24) by $(\theta_1 + 120°)$ and $(\theta_1 - 120°)$, respectively.

The remaining parameters to be determined are γ, ρ_1, and θ_1. As discussed in Sec. II, the apex angle γ is fixed by the choice of the translational lattice. Therefore, we utilize the remaining freedom in choosing ρ_1 and θ_1 in Eq. (24) to optimize the interference contrast *C* which is defined as the ratio of maximum to minimum exposure dose $(D_{\max}/D_{\min} = \tilde{D}_{\max}/\tilde{D}_{\min})$. *C* is a parameter of practical importance for the fabrication and largely determines the quality of the sample. In the present case, the exposure dose (9) takes on the form

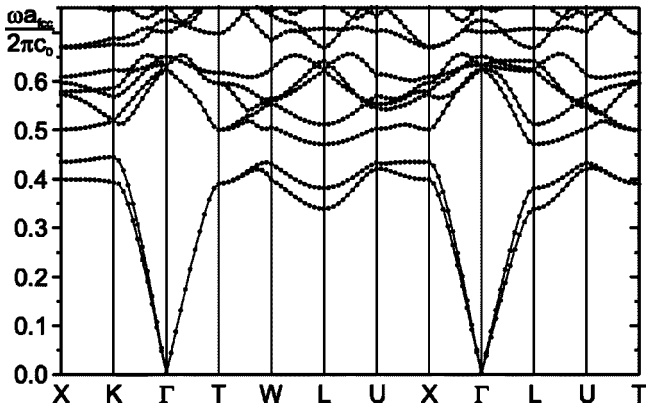

FIG. 3. Band structure of the rhombohedral photonic crystal corresponding to $(u,0,0,0)$, $\gamma = \gamma_{\text{fcc}}$, and $f_{\text{Si}} = 38\%$. The underlying Brillouin zone is illustrated in Fig. 6, the real-space crystal in Fig. 5.

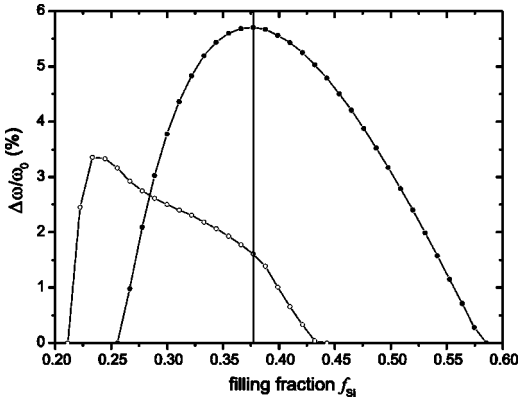

FIG. 4. Relative width of the gap versus filling fraction corresponding to the parameters used in Fig. 3. The dots refer to the fundamental gap and the open dots to the gap between the seventh and eighth band. The vertical line indicates the optimum filling fraction of $f_{\text{Si}} = 38\%$.

$$\tilde{D}(\vec{r}_r) \propto (a_{11} + a_{22} + a_{33} + a_{44}) + 2u[\cos(2\pi x_r) + \cos(2\pi y_r) + \cos(2\pi z_r)]. \quad (25)$$

This function varies by $\pm 6u$ around the bias value $(a_{11} + a_{22} + a_{33} + a_{44})$. Using Eq. (18), *C* becomes

$$C = \frac{\rho_1^2 + \rho_2^2 + \rho_3^2 + \rho_4^2 + 6u}{\rho_1^2 + \rho_2^2 + \rho_3^2 + \rho_4^2 - 6u}. \quad (26)$$

Figure 2 shows the contrast *C* as function of (ρ_1^2/u) and the deviation $\theta_1 - \theta_1^{\text{opt}}$ from the optimum polarization direction θ_1^{opt}. A sharp peak is clearly visible, corresponding to the optimal parameter values for maximal interference contrast.

Although the optimum angle θ_1^{opt} depends on the choice of the apex angle γ, the dependence of the contrast *C* on $\theta_1 - \theta_1^{\text{opt}}$ is universal. The optimum scaled intensity $(\rho_1^{\text{opt}})^2/u$ does also not depend on the apex angle γ.

The maximum contrast is reached for

$$\theta_1^{\text{opt}} = \text{arccot}\left(\frac{\cos(\gamma)}{\sqrt{3\sin^2(\gamma) - 1}}\right), \quad (27)$$

$$(\rho_1^{\text{opt}})^2/u = \left(\frac{27}{2}\right)^{1/2}, \quad (28)$$

which leads to corresponding intensities of the side beams

$$\rho_2^{\text{opt}} = \frac{-\rho_3^{\text{opt}}}{2} = \frac{-\rho_4^{\text{opt}}}{2} = \sqrt{u}\left(\frac{1}{6}\right)^{1/4}. \quad (29)$$

Remarkably, the values for ρ_n^{opt} $n = 2,3,4$ do not depend on the apex angle γ either. The corresponding polarization angles $\theta_{2,3,4}^{\text{opt}}$ are already fixed to $\theta_{2,3,4}$ according to Eq. (23).

With these parameters, we obtain for the optimum contrast (sc and fcc translational symmetry included) in the umbrella configuration

$$C^{\max}(\rho_1^{\text{opt}}, \theta_1^{\text{opt}}) = (\sqrt{6} + 2)/(\sqrt{6} - 2) \approx 9.90. \quad (30)$$

For sc and fcc, the optimized beam parameters are summarized in Table III. As discussed in Secs. II B 1, II B 2, and

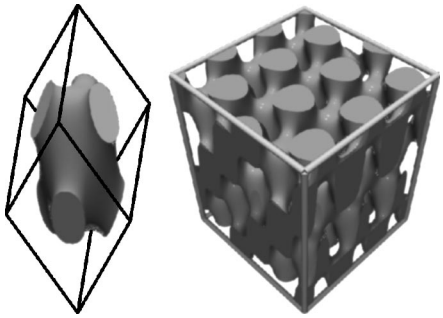

FIG. 5. Left: Motif of the structure according to Eq. (15) within the rhombohedral unit cell for a filling fraction of $f_{Si}=38\%$. Right: Fragment of the corresponding crystal structure.

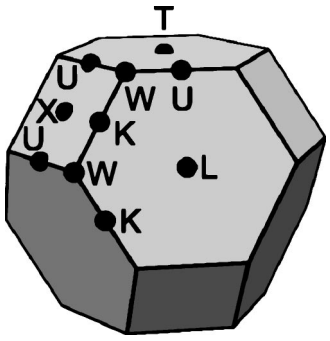

FIG. 6. High-symmetry points of the Brillouin zone of rhombohedral structures with fcc translational symmetry (Ref. 36).

II B 3 only the structure with fcc translational symmetry can actually be manufactured owing to its relatively small apex angle inside the photoresist which can be achieved through immersion techniques.

IV. BAND STRUCTURES

After discussing the crystallographic symmetries (see Appendix A for a graphical summary) and certain aspects about the fabrication of corresponding template structures, we are now in a position to investigate the photonic band structures that result when the templates are back filled with a high refractive index material. For these calculations, we assume that, in order to enhance the refractive index contrast, the polymer network is subsequently removed through a selective etching process. For given apex angle γ, the only remaining free parameters are the refractive index of the infiltrated material and its volume filling fraction f. The latter is equivalent to scaling the overall intensity of all four beams. We chose silicon as the high refractive index material ($n=\sqrt{11.9}$) for applications near the telecommunication wavelength of 1.5 μm. This choice is inspired by the successfull infilling of silicon into the voids of artificial opals.[4,5]

The search for PBG's and the corresponding optimum volume filling fraction f for maximum gap/midgap ratio is carried out using a plane-wave expansion method[34,35] using 1219 plane waves so that the results are converged to within less than 0.5% of their absolute value.

We consider only the cases of simple cubic and face-centered cubic translational symmetry. For the sc case, we find a complete PBG between the fifth and the sixth band with a gap/midgap ratio of just above 10% after silicon infiltration with an optimum filling fraction of $f_{Si}=24\%$. This is in excellent agreement with previous work.[19] For the fcc case, with rhombohedral space group symmetry, we find a complete PBG between the second and third band with a gap/midgap ratio of 58% after silicon back filling with an optimum filling fraction of $f_{Si}=38\%$ (see Fig. 3). This PBG remains open for filling fractions f_{Si} in an interval from 26 to 59% (see Fig. 4). The corresponding silicon PhC [$(u,0,0,0)$, $\gamma=\gamma_{fcc}$, and $f_{Si}=38\%$] is illustrated in Fig. 5. Its symmetry is identical to that of the celebrated Yablonovite structure,[31] the motif of which consists of three crossing rods of cylindrical or elliptical cross section. For our structure, the region where the rods intersect is somewhat thickened as compared to the Yablonovite. The corresponding rhombohedral Brillouin zone is depicted in Fig. 6. Owing to the rhombohedral overall symmetry, the irreducible Brillouin zone is larger than that of the standard fcc case and the nomenclature of the various characteristic points is different from that of the fcc irreducible Brillouin zone[36]. This lack of cubic symmetry is, for instance, manifest in the birefringence of the first two bands in the long wavelength limit, i.e., the splitting of the bands for low frequencies near the Γ point. Moreover, a closer inspection of Fig. 3 reveals that this structure exhibits a second PBG at higher frequencies between bands seven and eight. For this PBG, the maximum size of 3.4% is obtained at a silicon filling fraction of $f_{Si}=24\%$ and the PBG remains open for filling fractions f_{Si} between 21 and 43%. While this PBG might be rather sensitive to fabricational tolerances (similar to the PBG in inverse opals), we speculate that the fundamental PBG in this structure should be rather robust against disorder.

V. CONCLUSIONS

In summary, we have carried out a systematic investigation of the umbrella geometry for the fabrication of photonic crystal templates using holographic lithography. The attainable lattice constants using different beam geometries suggest that the umbrella configuration exhibits certain advantages when it comes to the actual fabrication of these templates. Our crystallographic analysis has revealed that the resulting structures are generally of rhombhedral symmetry and the most promising candidates for complete PBG's are structures with sc overall and fcc translational (and rhombohedral overall) symmetry, respectively. We have shown that both the sc and the fcc templates can in principle be fabricated as both yield interference contrast of the order of 10.

However, the large apex angle required for obtaining the sc structure will push the limits of the currently available immersion systems. In addition, the relatively small lattice constant $a_{sc}=0.87\lambda$ of the sc lattice makes this structure rather unattractive to applications in the near infrared. For the fcc translational structure (see Fig. 5), we have—to the best of our knowledge for the first time—determined parameters such as beam intensities and polarizations that (i) make

the structure experimentally feasible (attainable apex angle and lattice constant $a_{\mathrm{fcc}}=2.60\lambda$ suitable for telecommunication applications) and (ii) will lead to a complete PBG between the second and third band with a gap/midgap ratio of 5.8% after silicon inversion with 38% silicon by volume. This structure can be realized either with negative or positive photoresists (balanced structure) through single or double inversion, respectively. These results show that holographic lithography is a promising technique for the rapid, large-scale, flexible, and inexpensive fabrication of photoresist templates.

Note added in proof. C. K. Ullal *et al.*[38] have independently also found the solution with rhombohedral overall symmetry and fcc translational symmetry accessible via the umbrella geometry.

ACKNOWLEDGMENTS

We thank E.L. Thomas for providing us with a preprint of Ref. 20 prior to publication. We acknowledge support by the Deutsche Forschungsgemeinschaft through projects A1.1 and A1.4 of the DFG-Forschungszentrum "Functional Nanostructures." The research of K.B. is further supported by the DFG under Grant No. BU 1107/2-3 (Emmy-Noether program), that of M.W. by Project No. We1497/9-1.

APPENDIX A: GRAPHIC REPRESENTATION OF SYMMETRY ANALYSIS

In this appendix, we present a graphic representation (Fig. 7) of our symmetry analysis that illustrates the multitude of parameter choices in holographic lithography, only a few of which lead to structures that can actually be fabricated and that exhibit complete PBG's.

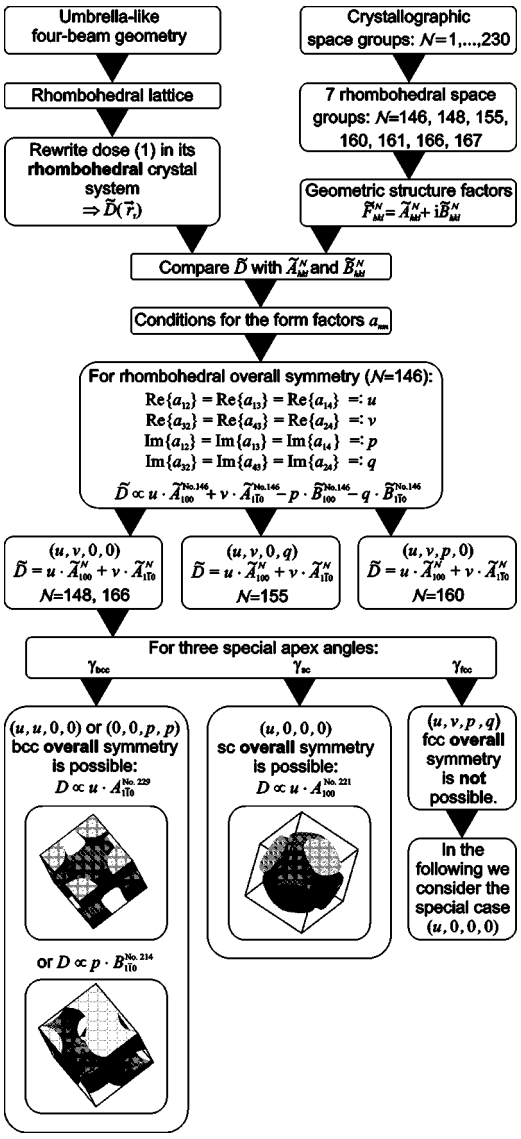

FIG. 7. Illustration and summary of our symmetry analysis (Ref. 37).

*Email address: daniel.meisel@physik.uni-karlsruhe.de

[1] S. John, Phys. Rev. Lett. **58**, 2486 (1987).
[2] E. Yablonovitch, Phys. Rev. Lett. **58**, 2059 (1987).
[3] J. E. G. J Wijnhoven and W. Vos, Science **281**, 802 (1998).
[4] A. Blanco, E. Chomski, S. Grabtchak, M. Ibisate, S. John, S. W. Leonard, C. Lopez, F. Meseguer, H. Miguez, J. P. Mondia, G. A. Ozin, O. Toader, and H. M. vanDriel, Nature (London) **405**, 437 (2000).
[5] Y. A. Vlasov, X.-Z. Bo, J. C. Sturm, and D. J. Norris, Nature (London) **414**, 289 (2001).
[6] K.-M. Ho, C. T. Chan, C. M. Soukoulis, R. Biswas, and M. Sigalas, Solid State Commun. **89**, 413 (1994).
[7] E. Özbay, A. Abeyta, G. Tuttle, M. Tringides, R. Biswas, C. T. Chan, C. M. Soukoulis, and K. M. Ho, Phys. Rev. B **50**, 1945 (1994).
[8] S. Y. Lin, J. G. Flemming, D. L. Hetherington, B. K. Smith, R. Biswas, K. M. Ho, M. M. Sigalas, W. Zubrzycki, S. R. Kurtz, and J. Bur, Nature (London) **394**, 251 (1998).
[9] S. Noda, K. Tomoda, N. Yamamoto, and A. Chutinan, Science **289**, 604 (2000).
[10] K. Aoki, H. T. Miyazaki, H. Hirayama, K. Inoshita, T. Baba, K. Sakoda, N. Shinya, and Y. Aoyagi, Nat. Mater. **2**, 117 (2003).
[11] M. Campbell, D. N. Sharp, M. T. Harrison, R. G. Denning, and A. J. Turberfield, Nature (London) **404**, 53 (2000).
[12] S. Shoji, and S. Kawata, Appl. Phys. Lett. **76**, 2668 (2000).
[13] Yu. V. Miklyaev, D. C. Meisel, A. Blanco, G. von Freymann, K. Busch, W. Koch, C. Enkrich, M. Deubel, and M. Wegener, Appl. Phys. Lett. **82**, 1284 (2003).
[14] M. Deubel, G. von Freymann, M. Wegener, S. Pereira, K. Busch, and C. M. Soukoulis, Nat. Mater. **3**, 444 (2004).

[15] K. I. Petsas, A. B. Coates, and G. Grynberg, Phys. Rev. A **50**, 5173 (1994).
[16] V. Berger, O. Gauthier-Lafaye, and E. Costard, J. Appl. Phys. **82**, 60 (1997).
[17] L. Z. Cai, X. L. Yang, and Y. R. Wang, Opt. Lett. **27**, 900 (2002).
[18] V. G. Minogin and J. Javanainen, Opt. Commun. **43**, 119 (1982).
[19] M. Maldovan, A. M. Urbas, N. Yufa, W. C. Carter, and E. L. Thomas, Phys. Rev. B **65**, 165123 (2002).
[20] C. K. Ullal, M. Maldovan, M. Wohlgemuth, and E. L. Thomas, J. Opt. Soc. Am. A **20**, 948 (2003).
[21] D. N. Sharp, A. J. Turberfield, and R. G. Denning, Phys. Rev. B **68**, 205102 (2003).
[22] O. Toader, T. Y. M. Chan, and S. John, Phys. Rev. Lett. **92**, 043905 (2004).
[23] L. Martín-Moreno, F. J. García-Vidal, and A. M. Somoza, Phys. Rev. Lett. **83**, 73 (1999).
[24] V. Babin, P. Garstecki, and R. Hołyst, Phys. Rev. B **66**, 235120 (2002).
[25] K. Michielsen and J. S. Kole, Phys. Rev. B **68**, 115107 (2003).
[26] *International Tables for Crystallography* (Kluwer, Dortdrecht, 1996), Vols. A and B.
[27] H. S. Sözüer and J. W. Haus, J. Opt. Soc. Am. B **10**, 296 (1993).
[28] H. A. Schwarz, *Gesammelte Mathematische Abhandlungen* (Springer, Berlin, 1890).
[29] M. Wohlgemuth, N. Yufa, J. Hoffman, and E. L. Thomas, Macromolecules **34**, 6083 (2001).
[30] A. H. Schoen, NASA Technical Note TN D-5541 (1970).
[31] E. Yablonovitch, T. JGmitter, and K. M. Leung, Phys. Rev. Lett. **67**, 2295 (1991).
[32] C. T. Chan, S. Datta, K. M. Ho, and C. M. Soukoulis, Phys. Rev. B **50**, 1988 (1994).
[33] W. Fischer and E. Koch, Z. Kristallogr. **179**, 31 (1987).
[34] K. M. Ho, C. T. Chan, and C. M. Soukoulis, Phys. Rev. Lett. **65**, 3152 (1990).
[35] K. Busch and S. John, Phys. Rev. E **58**, 3896 (1998).
[36] M. H. Cohen, Phys. Rev. **121**, 387 (1961).
[37] D. C. Meisel, M. Wegener, and K. Busch, *International Conference on Photonic and Electromagnetic Crystal Structures (PECS-V)*, Kyoto (Japan), March 7—11, 2004.
[38] C. K. Ullal, M Maldovan, E. L. Thomas, G. Chen, Y. -J. Han, and S. Yang, Appl. Phys. Lett. **84**, 5434 (2004).